

Monoaxial Dzyaloshinskii–Moriya interaction-induced topological Hall effect in a new chiral-lattice magnet GdPt₂B

Yoshiki J. Sato^{1,*}, Hikari Manako¹, Ryuji Okazaki¹, Yukio Yasui², Ai Nakamura³, and Dai Aoki³

¹*Department of Physics and Astronomy, Faculty of Science and Technology,
Tokyo University of Science, Noda, Chiba 278-8510, Japan*

²*School of Science and Technology, Meiji University, Kawasaki, Kanagawa 214-8571, Japan*

³*Institute for Materials Research, Tohoku University, Oarai, Ibaraki 311-1313, Japan*

(Dated: June 7, 2023)

We investigate the topological Hall effect (THE) in the monoaxial chiral crystal GdPt₂B, a recently discovered compound that exhibits putative helimagnetism below 87 K. The distinct THE was observed in GdPt₂B in the magnetically ordered state. The scaling relations for anomalous and topological Hall conductivities differed from those of conventional models based on the scattering process. We further demonstrate the clear scaling behavior of the THE in a wide temperature range, which we attribute to the monoaxial Dzyaloshinskii–Moriya (DM) interaction under external magnetic fields perpendicular to the screw axis. The THE induced by the monoaxial DM interaction as well as the THE in a monoaxial chiral crystal of *f*-electron system are demonstrated in this study.

I. INTRODUCTION

Chirality is an important concept across many natural sciences. In physics, the absence of mirror symmetry in matter plays a key role in chirality-induced phenomena [1–3]. In particular, an asymmetric exchange interaction, namely the Dzyaloshinskii–Moriya (DM) interaction [4, 5], arising from relativistic spin–orbit coupling (SOC), stabilizes chiral helimagnetism in magnetic materials with chiral crystal structures. The competition between an external magnetic field and magnetic interactions, including the DM interaction, induces characteristic spin textures, resulting in exotic spin-charge coupled phenomena such as the topological Hall effect (THE) [6–8] and electrical magnetochiral effect [9, 10].

In many studies on the magnetic and transport properties of chiral magnetic materials, B20-type cubic chiral compounds have been intensively investigated as archetypal chiral magnets [6–9, 11, 12]. They crystallize into the cubic space group $P2_13$ with four three-fold rotational axes. This peculiarity of multiple helical axes causes a complex interplay between the external magnetic field and the DM interaction, resulting in characteristic spin textures [8, 9, 11, 12] and complex responses to the direction of the magnetic field [8, 13, 14]. In contrast to the cubic system, hexagonal, tetragonal, and trigonal chiral crystals have one principal helical axis. They were classified as monoaxial chiral crystals.

Although a relatively large number of cubic chiral helimagnets have been reported [15], there are few known systems of monoaxial helimagnets with chiral crystal structures, such as intercalated transition metal dichalcogenides (TMDs) [16–18], CsCuCl₃ [19], and YbNi₃Al₉ [20]. In the monoaxial chiral crystals, the SOC causes “monoaxial” DM interaction along the screw axis [21]. The TMD magnet CrNb₃S₆ (space group $P6_322$) is an

intensively investigated monoaxial helimagnet that exhibits a chiral soliton lattice (CSL) phase under a magnetic field perpendicular to the monoaxial DM interaction [22]. The CSL exhibits strong coupling with conduction electrons and induces nontrivial magnetotransport [23, 24]. In addition, recent studies have shown a topological and planar Hall effect in the tilted CSL of a TMD [25] and transformations from a CSL to magnetic skyrmions in monoaxial TMD crystals with confined geometries [26]. However, the question of whether the monoaxial DM interaction directly causes spin-charge coupled phenomena is an important issue. We address this issue by exploring a novel monoaxial chiral crystal system.

In this paper, we report the emergence and robust scaling behavior of the THE in a monoaxial chiral crystal GdPt₂B, under a magnetic field perpendicular to the screw axis. In a series of CePt₂B type chiral materials [27–33], the *f*-electron based magnet GdPt₂B is a recently discovered compound, which crystallizes in a hexagonal chiral space group $P6_422$ [34]. The hexagonal crystal structure and schematic magnetic (*H*-*T*) phase diagram of GdPt₂B are shown in Figs. 1(a) and 1(b), respectively. GdPt₂B is a metallic compound and exhibits putative chiral helimagnetism below $T_O = 87$ K. The electrical resistivity ρ_{xx} , specific heat C_p , and magnetization M exhibit a distinct phase transition at T_O , as shown in Fig. 1(c). In addition, $M(T)$ shows a weak anomaly associated with spin reorientation at $T_{\chi_{\max}} \sim 50$ K. The Curie–Weiss analysis gives a positive Weiss temperature $\theta_W \sim 100$ K, indicating ferromagnetic exchange interaction between the Gd-ions. A distinct THE was observed in bulk single crystals of GdPt₂B subjected to an external magnetic field perpendicular to the screw axis (i.e., H was perpendicular to the direction of the monoaxial DM interaction). This phenomenon, arising from the competition between external magnetic fields and monoaxial DM interaction, has rarely been reported. We found the scaling behavior of the THE based on a 1-D Hamiltonian for monoaxial crystals. To the best of our knowledge, this is the first study to demonstrate the emergence of

* yoshiki_sato@rs.tus.ac.jp

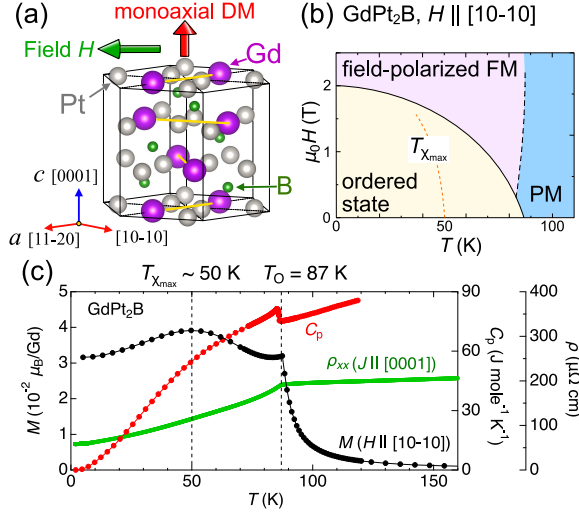


FIG. 1. (a) Crystal structure of GdPt₂B. (b) Schematic magnetic phase diagram consisting of ordered state, paramagnetic (PM), and field-polarized ferromagnetic (FM) phases. (c) Temperature dependence of magnetization $M(T)$, specific heat (C_p), and electrical resistivity (ρ). $\rho(T)$ and $C_p(T)$ were measured in zero field, and $M(T)$ was measured in a magnetic field of $\mu_0 H = 0.05$ T. $C_p(T)$ and $M(T)$ data were taken from Ref.[34].

the THE induced by the monoaxial DM interaction as well as the THE in f -electron based monoaxial chiral crystals.

II. EXPERIMENTAL DETAILS

Single crystals of GdPt₂B were grown using the Czochralski method in a tetra arc furnace. The single crystals of GdPt₂B were oriented using a Laue camera (Photonic Science Laue X-ray CCD camera). Hall measurements were performed using bulk single crystals cut into thin plates with dimensions of $1.5 \text{ mm} \times 1.5 \text{ mm} \times 0.1 \text{ mm}$. The longitudinal and Hall resistances were simultaneously measured using a lock-in amplifier (SR-830) in a physical property measurement system (PPMS). Magnetization measurements were performed using a superconducting quantum interference device magnetometer (MPMS).

III. RESULTS AND DISCUSSION

The observed Hall resistivity ρ_{yx}^{obs} of GdPt₂B for the magnetic field $H \parallel [10\bar{1}0]$ and electrical current $J \parallel [0001]$ at 50 K is shown in Fig. 2(a). Usually, the Hall resistivity is expressed as follows:

$$\rho_{yx} = \rho_{yx}^{\text{O}} + \rho_{yx}^{\text{A}} + \rho_{yx}^{\text{T}}. \quad (1)$$

The first term $\rho_{yx}^{\text{O}} = R_0 B$ is the ordinary Hall effect (OHE) due to the Lorentz force, and R_0 is the ordinary

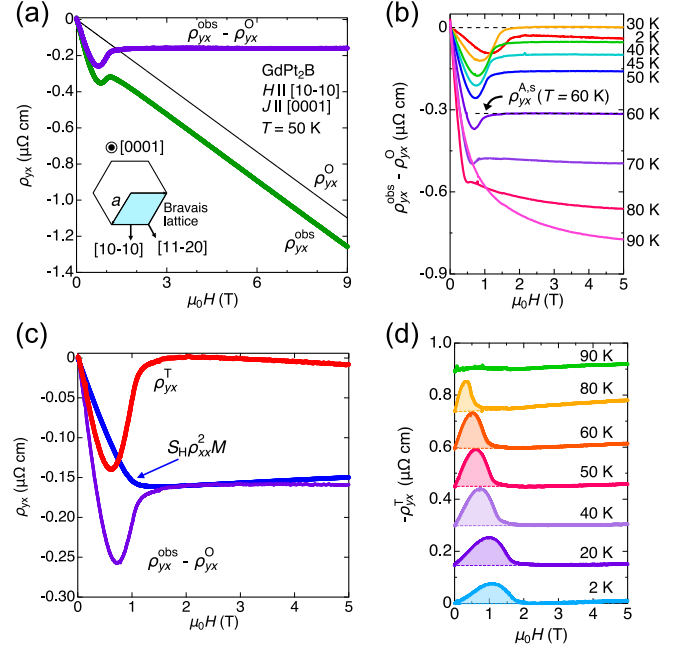


FIG. 2. (a) Field dependence of anomalous Hall resistivity ρ_{yx}^{A} after subtraction of ordinary Hall resistivity ρ_{yx}^{O} from observed Hall resistivity ρ_{yx}^{obs} at 50 K. (b) $\rho_{yx}^{\text{obs}} - \rho_{yx}^{\text{O}}$ at several constant temperatures. (c) Topological Hall resistivity ρ_{yx}^{T} after subtraction of anomalous Hall component derived from the magnetization ($\rho_{yx}^{\text{A}} = S_H \rho_{xx}^2 M$). (d) Extracted $-\rho_{yx}^{\text{T}}$ at several constant temperatures.

Hall coefficient. The second term ρ_{yx}^{A} is the anomalous Hall effect (AHE) derived from the magnetization of the sample. The third term ρ_{yx}^{T} is the topological Hall resistivity induced by topological spin textures. In a high field region, the linear field dependence of ρ_{yx}^{obs} of GdPt₂B can be interpreted as the ordinary Hall effect ρ_{yx}^{O} .

The field dependence of the Hall component after removing the ordinary Hall effect, namely $\rho_{yx}^{\text{obs}} - \rho_{yx}^{\text{O}}$, is shown in Figs. 2(a) and 2(b). A clear hump-like anomaly was observed. To extract the topological Hall component, we estimated the anomalous Hall effect corresponding to the magnetization of the sample. Generally, the anomalous Hall resistivity is described as [35, 36]:

$$\rho_{yx}^{\text{A}} = \alpha \rho_{xx}(H)M(H) + S_H \rho_{xx}^2(H)M(H), \quad (2)$$

where α and S_H are material specific constants. The first and second terms correspond to skew scattering and intrinsic (Berry phase) contributions, respectively. As shown in Fig. 2(c), the field dependence of ρ_{yx}^{A} can be reasonably explained by the intrinsic contribution $S_H \rho_{xx}^2(H)M(H)$ in the field-polarized FM state. Here, the $M(H)$ data were corrected using the demagnetizing factor $D_z \sim 0.8$ for precise analysis [37] (see Supplemental Material (SM) for details [38]). The fact that ρ_{yx}^{A} can be well explained by assuming an intrinsic contribution above T_0 indicates the validity of the current analysis (see SM [38]).

The extracted topological Hall resistivity, namely $\rho_{yx}^T(H) = \rho_{yx}^{\text{obs}}(H) - \rho_{yx}^O(H) - \rho_{yx}^A(H)$, is shown in Figs. 2(c) and 2(d). The hump-like field dependence of ρ_{yx}^T resembles the Hall effect induced by topological spin textures such as skyrmion lattices in B20 chiral helimagnets [6, 7, 39]. The topological Hall resistivity of GdPt₂B is negative and reaches a maximum value of $|\rho_{yx}^T| = 0.14 \mu\Omega\text{cm}$ at $T = 45 \text{ K}$. The order of magnitude of ρ_{yx}^T is comparable to the reported values of topological Hall resistivity of MnGe ($\sim 0.16 \mu\Omega\text{cm}$ [7]) and EuPtSi ($\sim 0.12 \mu\Omega\text{cm}$ [39]). As shown in Fig. 2(d), the hump-like anomaly in ρ_{yx}^T vanishes above the transition temperature T_O , suggesting that the magnetically ordered state and the spin chirality are closely related to the emergence of the THE in GdPt₂B.

Here, we discuss the scaling relation for AHE between σ_{yx}^A and σ_{xx} arising from the scattering mechanism. Figure 3(a) shows a log-log plot of $|\sigma_{yx}^A|$ versus σ_{xx} . σ_{yx}^A is defined as $(-\rho_{yx}^A)/[(\rho_{yx}(H_s)^2 + \rho_{xx}(H_s)^2)]$, where ρ_{yx}^A is the saturation value of $\rho_{yx}^{\text{obs}} - \rho_{yx}^O$ in a field of H_s [see Fig. 2(b)]. σ_{xx} is calculated as $[\rho_{xx}(H_s)]/[\rho_{yx}(H_s)^2 + \rho_{xx}(H_s)^2]$. In a "bad metal" regime with a small longitudinal conductivity, the scaling law $\sigma_{yx} \propto \sigma_{xx}^{1.6}$ has been demonstrated in several materials [40–43]. In contrast, σ_{yx} becomes nearly constant in the intermediate regime ($\sigma_{xx} \sim 10^4$ to $10^6 \Omega^{-1}\text{cm}^{-1}$ [41, 42]). The data for GdPt₂B and several other compounds are plotted in Fig. 3(a). The scaling plot suggests that GdPt₂B is in the intermediate regime, but the scaling behavior of the AHE in GdPt₂B exhibits a peculiar temperature dependence.

At the lowest temperature (2 K), $|\sigma_{yx}^A|$ is approximately $12 \Omega^{-1}\text{cm}^{-1}$ with a saturation magnetic moment M_{sat} of $7.2 \mu_B/\text{Gd}$. As the temperature increases, $|\sigma_{yx}^A|$ shows a minimum value of $|\sigma_{yx}^A| = 0.2 \Omega^{-1}\text{cm}^{-1}$ ($M_{\text{sat}} = 6.5 \mu_B/\text{Gd}$) at 30 K and reaches a nearly constant value of $|\sigma_{yx}^A| \sim 25 \Omega^{-1}\text{cm}^{-1}$ ($M_{\text{sat}} = 4.3 \mu_B/\text{Gd}$) above 60 K. M_{sat} and magnetoresistance vary systematically in the high field region. Therefore, the temperature dependence of the AHE in GdPt₂B cannot be explained by conventional AHE scenarios. The breakdown of the scaling relation of AHE is an interesting phenomenon. The mechanisms such as electron-phonon scattering[46] and Kondo coherence in an *f*-electron system[47] have recently been discussed as the origin of the breakdown of the scaling relation. The mechanism underlying the peculiar scaling behavior of AHE in GdPt₂B remains unclear.

Figure 3(b) shows the temperature dependence of the coefficients R_0 and $-S_H$, together with the maximum value of topological Hall resistivity $|\rho_{yx}^T|_{\text{max}}$. Whereas, the THE of GdPt₂B is rapidly suppressed in the PM and field-polarized FM states, and the OHE and AHE exhibit a smooth temperature dependence near T_O . R_0 was negative at all measured temperatures, indicating that the electron is a dominant carrier. The charge carrier density n is estimated to be $n = 5.74 \times 10^{27} \text{ m}^{-3}$ and $n =$

$4.20 \times 10^{27} \text{ m}^{-3}$ at 80 and 2 K, respectively. R_0 takes its maximum value near T_O . The coefficient $-S_H$ exhibits a weak temperature dependence near T_O and reaches its maximum value at $T = 110 \text{ K}$. $|\rho_{yx}^T|_{\text{max}}$ peaks near $T_{\chi_{\text{max}}} \sim 50 \text{ K}$.

In order to elucidate the origin of THE in GdPt₂B, we examined the field dependence of topological Hall conductivity σ_{yx}^T for $H \parallel [10\bar{1}0]$ at several constant temperatures, as shown in Fig. 4(a). σ_{yx}^T is calculated as $[-\rho_{yx}^T(H)]/[\rho_{yx}(H)^2 + \rho_{xx}(H)^2]$. The maximum value of σ_{yx}^T reaches $21 \Omega^{-1}\text{cm}^{-1}$ at 2 K and decreases with increasing temperature.

The THE exhibits different scattering time τ dependence depending on its mechanism, in conventional scenarios[7, 48–50]. In the case of the intrinsic mechanism due to the momentum-space Berry curvature, the anomalous Hall component is independent of τ [41, 42]. In contrast, σ^T is expected to show τ^2 dependence in the case of the THE induced by topological spin textures such as magnetic skyrmions because a fictitious magnetic flux in real space is proportional to the number of topological spin textures in a given area [48, 50, 51]. We plot extreme values of σ_{yx}^T as a function of σ_{xx} in Fig. 4(b), where σ_{xx} is proportional to τ under the assumption that n and the effective mass of the carrier are constant. The τ dependence of the topological Hall conductivity of GdPt₂B differs from those of conventional models based on momentum-space and real-space Berry curvatures. From the power-law fitting, we found that the extreme value of σ_{yx}^T is proportional to $1/\sqrt{\tau}$ in GdPt₂B. A previous theoretical study explored the τ dependence of the length of the topological spin texture L_s^* , which correspond to the length where σ_{yx}^T reaches its extreme value [52]. For short-pitch skyrmion lattices, it was verified that L_s^* is proportional to $\sqrt{\tau}$ instead of the conventional τ dependence because of the band separation in the magnetic Brillouin zone [52]. The nontrivial $1/\sqrt{\tau}$ dependence of the THE in GdPt₂B may be attributed to the specific period and configuration of the spin texture.

The most salient feature of the THE in GdPt₂B is that its mechanism is closely related to the monoaxial DM interaction. To discuss the connection between the THE and monoaxial DM interaction, we first define H_{max}^T as the magnetic field corresponding to the maximum value of σ_{yx}^T . Figure 4(c) shows the critical field of the ordered state H_c as a function of H_{max}^T , exhibiting a linear relationship. Thus, the ratio of H_c to H_{max}^T remained constant, as shown in Fig. 4(d). Remarkably, the relationship between H_c and H_{max}^T holds for the entire temperature range below T_O .

To discuss the origin of the constant ratio H_c/H_{max}^T , we consider a simple 1-D Hamiltonian [21] for monoaxial crystal systems as follows:

$$\mathcal{H} = -J \sum_i \mathbf{S}_i \cdot \mathbf{S}_{i+1} - D \cdot \sum_i \mathbf{S}_i \times \mathbf{S}_{i+1} + \mathbf{H} \cdot \sum_i \mathbf{S}_i, \quad (3)$$

where \mathbf{S}_i ($|\mathbf{S}_i| = S$) is the local moment at site i , J is the ferromagnetic exchange interaction between two adjacent

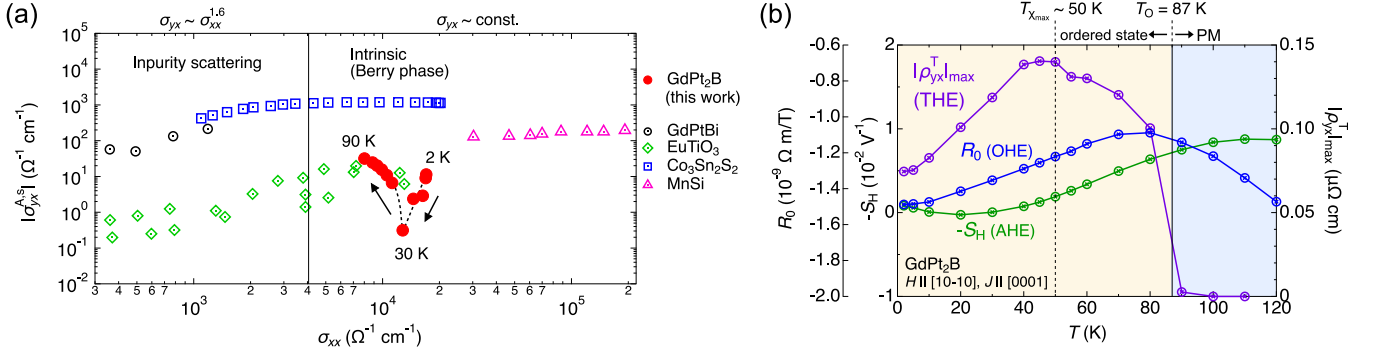


FIG. 3. (a) Scaling relations between the Hall conductivity $|\sigma_{yx}^{A,s}|$ and the longitudinal conductivity σ_{xx} for GdPt₂B and several compounds [43–45]. (b) Temperature dependence of coefficients R_0 , $-S_H$, and maximum value of $|\rho_{yx}^T|$.

spins, and \mathbf{D} ($|\mathbf{D}| = D$) is the monoaxial DM interaction along the screw axis. The third term represents the effect of the external magnetic field perpendicular to the screw axis. Based on the above 1-D Hamiltonian, Kishine and Ovchinnikov derived H_c as follows [21]:

$$H_c = \left(\frac{\pi}{4}\right)^2 S \frac{D^2}{J}. \quad (4)$$

Equation (4) indicates that the H_c is a measure of the ratio of monoaxial DM interaction D and the ferromagnetic exchange interaction J . Therefore, the constant ratio of H_c/H_{max}^T suggests that the THE of GdPt₂B attains its maximum values at a specific ratio of D^2/J and the external magnetic field perpendicular to the screw axis. The observed THE could be scaled by the critical field H_c . Figure 4(e) shows the normalized topological Hall conductivity $\sigma_{yx}^T/\sigma_{yx,\text{extrm}}^T$ as a function of the scaled external magnetic field H/H_c . The observed robust scaling behavior indicates that the monoaxial DM interaction plays a significant role in the emergence of THE in the monoaxial chiral crystal GdPt₂B.

To summarize the results of the THE in GdPt₂B, we show a contour plot of the topological Hall conductivity in the H - T phase diagram, as shown in Fig. 4(f). An important feature is that the THE of GdPt₂B is stable at the lowest temperature (2 K), without the influence of thermal agitations as observed in the DM-mediated skyrmions in chiral magnets. A distinct THE is observed only within the ordered state, and the extreme value of σ_{yx}^T depends on the scattering time. The results indicate that the spin texture in the ordered state is related to the emergence of the THE. In addition, H_c and H_{max}^T show a constant ratio below T_0 , suggesting the importance of the monoaxial DM interaction in the THE. It is noteworthy that the scalar spin chirality $[\mathbf{S}_i \cdot (\mathbf{S}_j \times \mathbf{S}_k)]$ vanishes in coplanar spin configurations such as the simple helimagnetism and CSL. Recent studies have discussed novel mechanisms such as the noncolinear Hall effect in coplanar spin configurations [53]. Magnetic structure analysis is a desirable next step in determining the microscopic origin of the monoaxial DM interaction-induced THE in

GdPt₂B.

Finally, we compare the THE in GdPt₂B with those in other material systems. In Gd-based centrosymmetric magnets such as Gd₂PdSi₃ [54, 55] and Gd₃Ru₄Al₁₂ [56], a large THE induced by the magnetic frustration in a hexagonal crystal has been reported. The Ruderman–Kittel–Kasuya–Yosida (RKKY) interaction produces modulated spin textures including the skyrmion lattice with three spiral spin modulations, that is, the triple- \mathbf{q} state. Owing to the complex magnetic interactions, the THE in Gd-based frustrated magnets is observed only in the intermediate magnetic phase, which is different from the present case for GdPt₂B. The dominant exchange interaction is considered to be of the RKKY type in GdPt₂B. The comparison of the THE in Gd-based monoaxial chiral crystal with those in centrosymmetric Gd-based magnets is important for a better understanding of the role of the DM interaction and mechanisms of THE. The present result is the first observation of the THE in a monoaxial chiral crystal of f -electron system, to the best of our knowledge. Another interesting example is large THE [25] and AHE [57] in the intercalated TMDs under the external magnetic fields along the helical axis. In the monoaxial chiral helimagnet CrNb₃S₆, a large THE induced by a tilted CSL state has been reported for $H \parallel c$ (helical axis). In general, the magnetic field along the helical axis leads to a simple conical structure; however, the monoaxial DM interaction may be effective for $H \parallel$ helical axis. The anisotropy of the THE in monoaxial chiral crystals needs to be clarified in the future.

IV. CONCLUSIONS

In conclusion, the large and distinct THE was observed in the monoaxial chiral crystal GdPt₂B. The characteristic τ dependence of the extreme value of σ_{yx}^T and the constant ratio of H_c/H_{max}^T lead to the clear scaling behavior of the topological Hall conductivity, indicating that the THE in GdPt₂B was induced by the monoaxial DM inter-

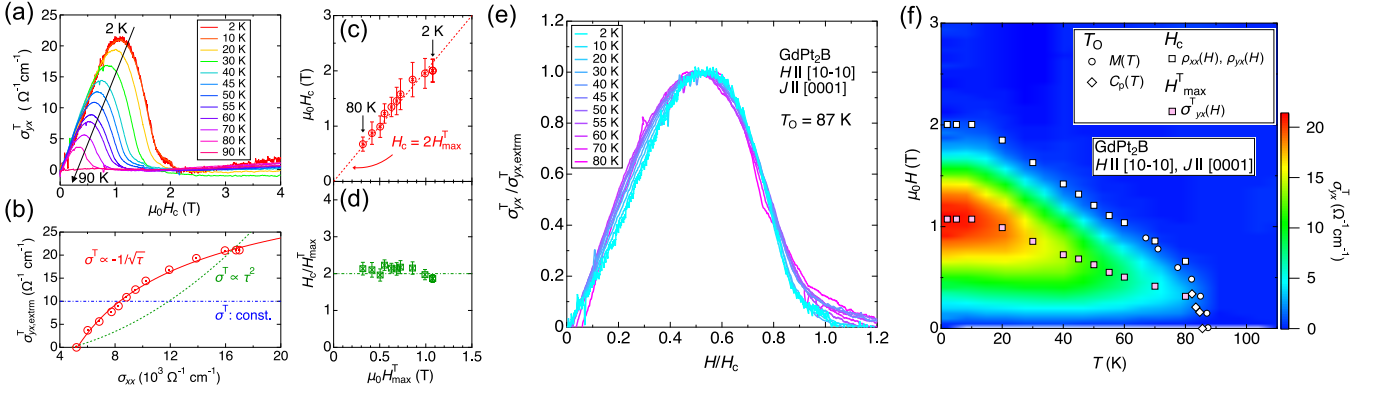


FIG. 4. (a) Topological Hall conductivity σ_{yx}^T as a function of magnetic field. (b) Scaling plot of extreme value of $\sigma_{yx}^T(H, T)$ as a function of $\sigma_{xx}(H, T)$. (c) The critical field H_c as a function of the magnetic field H_{\max}^T , which corresponds to $\sigma_{yx, \text{extrm}}^T$. (d) The ratio of H_c to H_{\max}^T . (e) Scaled topological Hall conductivity $\sigma_{yx}^T/\sigma_{yx, \text{extrm}}^T$ as a function of the scaled external magnetic field H/H_c . (f) Contour plot of σ_{yx}^T in the magnetic phase diagram of GdPt₂B for $H \parallel [10\bar{1}0]$.

action under external magnetic fields. The THE induced by the monoaxial DM interaction and THE in a monoaxial chiral crystal of f -electron system were demonstrated in this study. Our findings extend the range of material system in which the THE can be observed, and demonstrate the universal nature of the spin-charge coupled phenomena in topological materials.

ACKNOWLEDGMENTS

We would like to thank S. Ohara, S. Nakamura, and Y. Yamane for discussions. This work was supported

by JSPS KAKENHI (JP22K20360). We acknowledge all support from the International Research Center for Nuclear Materials Science at Oarai (IMR, Tohoku University).

-
- [1] G. L. J. A. Rikken and E. Raupach, *Nature* **390**, 493 (1997).
 - [2] B. Göhler, V. Hamelbeck, T. Z. Markuys, M. Kettner, G. F. Hanne, Z. Vager, R. Naaman, and H. Zacharias, *Science* **331**, 894 (2011).
 - [3] K. Shiota, A. Inui, Y. Hosaka, R. Amano, Y. Ōnuki, M. Hedo, T. Nakama, D. Hirobe, J.-I. Ohe, J.-I. Kishine, H. M. Yamamoto, H. Shishido, and Y. Togawa, *Phys. Rev. Lett.* **127**, 126602 (2021).
 - [4] I. Dzyaloshinsky, *J. Phys. Chem. Solids* **4**, 241 (1958).
 - [5] T. Moriya, *Phys. Rev.* **120**, 91 (1960).
 - [6] A. Neubauer, C. Pfleiderer, B. Binz, A. Rosch, R. Ritz, P. G. Niklowitz, and P. Böni, *Phys. Rev. Lett.* **102**, 186602 (2009).
 - [7] N. Kanazawa, Y. Onose, T. Arima, D. Okuyama, K. Ohoyama, S. Wakimoto, K. Kakurai, S. Ishiwata, and Y. Tokura, *Phys. Rev. Lett.* **106**, 156603 (2011).
 - [8] N. Nagaosa and Y. Tokura, *Nature Nanotech.* **8**, 899 (2013).
 - [9] T. Yokouchi, N. Kanazawa, A. Kikkawa, D. Morikawa, K. Shibata, T. Arima, Y. Taguchi, F. Kagawa, and Y. Tokura, *Nat. Commun.* **8**, 866 (2017).
 - [10] R. Aoki, Y. Kousaka, and Y. Togawa, *Phys. Rev. Lett.* **122**, 057206 (2019).
 - [11] S. Mühlbauer, B. Binz, F. Jonietz, C. Pfleiderer, A. Rosch, A. Neubauer, R. Georgii, and P. Böni, *Science* **323**, 915 (2009).
 - [12] X. Z. Yu, Y. Onose, N. Kanazawa, J. H. Park, J. H. Han, Y. Matsui, N. Nagaosa, and Y. Tokura, *Nature* **465**, 901 (2010).
 - [13] W. Münzer, A. Neubauer, T. Adams, S. Mühlbauer, C. Franz, F. Jonietz, R. Georgii, P. Böni, B. Pedersen, M. Schmidt, A. Rosch, and C. Pfleiderer, *Phys. Rev. B* **81**, 041203(R) (2010).
 - [14] T. Takeuchi, M. Kakihana, T. Nakama, and Y. Ōnuki, *J. Phys. Soc. Jpn.* **89**, 093703 (2020).
 - [15] Y. Tokura and N. Kanazawa, *Chem. Rev.* **121**, 2857 (2021).
 - [16] T. Miyadai, K. Kikuchi, H. Kondo, S. Sakka, M. Arai, and Y. Ishikawa, *J. Phys. Soc. Jpn.* **52**, 1394 (1983).
 - [17] S. K. Karna, F. N. Womack, R. Chapai, D. P. Young, M. Marshall, W. Xie, D. Graf, Y. Wu, H. Cao, L. DeBeer-Schmitt, P. W. Adams, R. Jin, and J. F. DiTusa, *Phys. Rev. B* **100**, 184413 (2019).
 - [18] C. Zhang, J. Zhang, C. Liu, S. Zhang, Y. Yuan, P. Li, Y. Wen, Z. Jiang, B. Zhou, Y. Lei, D. Zheng, C. Song, Z. Hou, W. Mi, U. Schwingenschlögl, A. Manchon, Z. Q. Qiu, H. N. Alshareef, Y. Peng, and X.-X. Zhang, *Adv.*

- Mater. **33**, 2101131 (2021).
- [19] Y. Kousaka, T. Koyama, K. Ohishi, K. Kakurai, V. Hutanu, H. Ohsumi, T. Arima, A. Tokuda, M. Suzuki, N. Kawamura, A. Nakao, T. Hanashima, J. Suzuki, J. Campo, Y. Miyamoto, A. Sera, K. Inoue, and J. Akimitsu, Phys. Rev. Mater. **1**, 071402(R) (2017).
 - [20] R. Miyazaki, Y. Aoki, R. Higashinaka, H. Sato, T. Yamashita, and S. Ohara, Phys. Rev. B **86**, 155106 (2012).
 - [21] J.-I. Kishine and A. S. Ovchinnikov, Solid State Phys. **66**, 1 (2015).
 - [22] Y. Togawa, T. Koyama, K. Takayanagi, S. Mori, Y. Kousaka, J. Akimitsu, S. Nishihara, K. Inoue, A. S. Ovchinnikov, and J. Kishine, Phys. Rev. Lett. **108**, 107202 (2012).
 - [23] Y. Togawa, Y. Kousaka, S. Nishihara, K. Inoue, J. Akimitsu, A. S. Ovchinnikov, and J. Kishine, Phys. Rev. Lett. **111**, 197204 (2013).
 - [24] Y. Togawa, Y. Kousaka, K. Inoue, and J.-I. Kishine, J. Phys. Soc. Jpn. **85**, 112001 (2016).
 - [25] D. A. Mayoh, J. Bouaziz, A. E. Hall, J. B. Staunton, M. R. Lees, and G. Balakrishnan, Phys. Rev. Research **4**, 013134 (2022).
 - [26] L. Li, D. Song, W. Wang, F. Zheng, A. Kovács, M. Tian, R. E. D.-Borkowski, and H. Du, Adv. Mater. , 2209798 (2023), <https://doi.org/10.1002/adma.202209798>.
 - [27] O. Sologub, P. Salamakha, H. Noël, M. Potel, M. Almeida, and C. Godart, J. Alloys. Compd. **307**, 40 (2000).
 - [28] O. L. Sologub, K. Hiebl, and P. S. Salamakha, Solid State Commun. **127**, 379 (2003).
 - [29] R. Lackner, M. Sieberer, H. Michor, G. Hilscher, E. Bauer, P. S. Salamakha, O. L. Sologub, and K. Hiebl, J. Phys.: Condens. Matter **17**, S905 (2005).
 - [30] M. Dias, O. L. Sologub, L. C. J. Pereira, and A. P. Gonçalves, J. Alloys. Compd. **438**, 62 (2007).
 - [31] R. T. Khan, G. Hilscher, H. Michor, E. Bauer, O. Sologub, P. Rogl, and G. Giester, J. Phys. Conf. Series **200**, 032034 (2010).
 - [32] R. T. Khan, F. Kneidinger, G. Hilscher, A. Sidorenko, O. Sologub, H. Michor, E. Bauer, P. Rogl, and G. Giester, J. Phys.: Condens. Matter **27**, 146001 (2015).
 - [33] Y. J. Sato, F. Honda, A. Maurya, Y. Shimizu, A. Nakamura, Y. Homma, D. X. Li, Y. Haga, and D. Aoki, Phys. Rev. Mater. **5**, 034411 (2021).
 - [34] Y. J. Sato, H. Manako, Y. Homma, D. X. Li, R. Okazaki, and D. Aoki, Phys. Rev. Mater. **6**, 104412 (2022).
 - [35] N. Nagaosa, J. Sinova, S. Onoda, A. H. MacDonald, and N. P. Ong, Rev. Mod. Phys. **82**, 1539 (2010).
 - [36] N. A. Porter, J. C. Gartside, and C. H. Marrows, Phys. Rev. B **90**, 024403 (2014).
 - [37] A. Aharoni, J. Appl. Phys. **83**, 3432 (1998).
 - [38] See Supplemental Material for description of the sample preparation, experimental method, analysis of the Hall effect and magnetoresistance.
 - [39] M. Kakihana, D. Aoki, A. Nakamura, F. Honda, M. Nakashima, Y. Amako, S. Nakamura, T. Sakakibara, M. Hedo, T. Nakama, and Y. Ōnuki, J. Phys. Soc. Jpn. **87**, 023701 (2018).
 - [40] W.-L. Kee, S. Watauchi, V. L. Miller, R. J. Cava, and N. P. Ong, Science **303**, 1647 (2004).
 - [41] T. Miyasato, N. Abe, T. Fujii, A. Asamitsu, S. Onoda, Y. Onose, N. Nagaosa, and Y. Tokura, Phys. Rev. Lett. **99**, 086602 (2007).
 - [42] S. Onoda, N. Sugimoto, and N. Nagaosa, Phys. Rev. B **77**, 165103 (2008).
 - [43] K. S. Takahashi, H. Ishizuka, T. Murata, Q. Y. Wang, Y. Tokura, N. Nagaosa, and M. Kawasaki, Sci. Adv. **4**, eaar7880 (2018).
 - [44] T. Suzuki, R. Chisnell, A. D. an Y.-T. Liu, W. Feng, D. Xiao, J. W. Lynn, and J. G. Checkelsky, Nat. Phys. **12**, 1119 (2016).
 - [45] E. Liu, Y. Sun, N. Kumar, L. Muechler, A. Sun, L. Jiao, S.-Y. Yang, D. Liu, A. Liang, Q. Xu, J. Kroder, V. Stüß, H. Borrmann, C. Shekhar, Z. Wang, C. Xi, W. Wang, W. Schnelle, S. Wirth, Y. Chen, S. T. B. Goennenwein, and C. Felser, Nat. Phys. **14**, 1125 (2018).
 - [46] C. Xiao, H. Zhou, and Q. Niu, Phys. Rev. B **100**, 161403(R) (2019).
 - [47] H. Siddiquee, C. Broyles, E. Kotta, S. Liu, S. Peng, T. Kong, B. Kang, Q. Zhu, Y. Lee, L. Ke, H. Weng, J. D. Denlinger, L. A. Wray, and S. Ran, Nat. Commun. **14**, 527 (2023).
 - [48] M. Onoda, G. Tatara, and N. Nagaosa, J. Phys. Soc. Jpn. **73**, 2624 (2004).
 - [49] Y. Shiomi, S. Iguchi, and Y. Tokura, Phys. Rev. B **86**, 180404(R) (2012).
 - [50] N. Verma, Z. Addison, and M. Randeria, Sci. Adv. **8**, eabq2765 (2022).
 - [51] P. Bruno, V. K. Dugaev, and M. Taillefumier, Phys. Rev. Lett. **93**, 096806 (2004).
 - [52] A. Matsui, T. Nomoto, and R. Arita, Phys. Rev. B **104**, 174432 (2021).
 - [53] J. Bouaziz, H. Ishida, S. Lounis, and S. Blügel, Phys. Rev. Lett. **126**, 147203 (2021).
 - [54] S. R. Saha, H. Sugawara, T. D. Matsuda, H. Sato, R. Mallik, and E. V. Sampathkumaran, Phys. Rev. B **60**, 12162 (1999).
 - [55] T. Kurumaji, T. Nakajima, M. Hirschberger, A. Kikkawa, Y. Yamasaki, H. Sagayama, H. Nakao, Y. Taguchi, T.-H. Arima, and Y. Tokura, Science **365**, 914 (2019).
 - [56] M. Hirschberger, T. Nakajima, S. Gao, L. Peng, A. Kikkawa, T. Kurumaji, M. Kriener, Y. Yamasaki, H. Sagayama, H. Nakao, K. Ohishi, K. Kakurai, Y. Taguchi, X. Yu, T.-H. Arima, and Y. Tokura, Nat. Commun. **10**, 5831 (2019).
 - [57] N. J. Ghimire, A. S. Botana, J. S. Jiang, J. Zhang, Y.-S. Chen, and J. F. Mitchell, Nat. Commun. **9**, 3280 (2018).